RSC Advances

ROYAL SOCIETY OF CHEMISTRY

www.rsc.org/advances

Highly stable organic-inorganic junction composed of hydrogenated titania nanotubes infiltrated by conducting polymer

Katarzyna Siuzdak[a], Mariusz Szkoda[b], Anna Lisowska-Oleksiak[b], Jakub Karczewski[c], Jacek Ryl[d]

[a] Centre for Plasma and Laser Engineering, Szewalski Institute of Fluid Flow Machinery, Polish Academy of Science, Fiszera 14, Gdańsk 80-231, Poland; Fax: +48 58 3416144; Tel: +48 58 6995294; *e-mail: ksiuzdak@imp.gda.pl

[b] Department of Chemistry and Technology of Functional Materials, Chemical Faculty, Gdańsk University of Technology, Narutowicza 11/12, Gdańsk 80-233, Poland

[c] Faculty of Applied Physics and Mathematics, Gdańsk University of Technology, Narutowicza 11/12, 80-233 Gdańsk, Poland

[d] Department of Electrochemistry, Corrosion and Materials Engineering, Gdańsk University of Technology, Narutowicza 11/12, 80-233 Gdańsk, Poland

ABSTRACT

In this study, poly(3,4-ethylenedioxythiophene) conducting polymer doped with poly(2-styrene sulphonate) (pEDOT:PSS) was efficiently electrodeposited on a layer composed of ordered titania nanotubes. TiO_2 nanotubes were formed during an anodization process and after calcination a layer was subjected to hydrogen plasma. Hydrogenation leads to Ti(III) formation, a decrease in resistance and a huge increase of donor density when compared to pure titania. According to a detailed structure analysis, the coverage by polymer matrix is uniform on the entire titania surface as well as along the tubes. Composite material exhibits highly enhanced anodic photocurrent (106 μA cm^{-2}) when compared to hydrogenated titania H-TiO_2 (54 μA cm^{-2}) or pure polymer film (2 μA cm^{-2}). Moreover, H-TiO_2/pEDOT:PSS is characterized with high photostability displayed during prolonged illumination. Proposed hydrogenation approach could be regarded as facile titania modification for further electrochemical modifications.

KEYWORDS: *H-TiO_2/pEDOT:PSS, photostability, plasma treatment, potentiostatic polymerization*

INTRODUCTION

Low-cost semiconducting materials and facile preparation of photovoltaic junctions constitute long-standing goals of photoactive materials research. Among many inorganic semiconductors, titanium dioxide, especially the well-ordered TiO_2 nanotubes (TiO_2NTs), have attracted a great deal of attention due to their key advantages: efficient pathway for vectorial electron transfer, light propagation through the nanoarchitecture and a large surface to volume area.[1,2] The ordered titania nanotubes are formed via electrochemical anodization of Ti plate immersed in fluoride-rich electrolyte. The precise optimization of anodization parameters, such as voltage, process duration, current distribution, temperature and electrolyte composition, allows to control the morphology of obtained TiO_2NTs film.[3] Owing to relatively simple and highly controlled anodization procedure, TiO_2 nanotubes replace TiO_2 nanoparticles in many applications. As n-type semiconductor, TiO_2NTs are widely used in sensors, electrochromic devices[4], as well as devices for energy conversion and storage.[5] In the case of photoconversion devices, titanium dioxide is widely used in dye-sensitized solar cells, inverted organic as a buffer layer[6] and blended with organic sensitized or donors.[7] In the TiO_2/polymer based solar cell, TiO_2 forms p-n heterojunctions where conducting polymer act as a p-element. Highly ordered heterojunctions obtained by filling metal oxide nanostructure with conducting polymer have distinctive advantages over composite when nanoparticles are randomly distributed inside polymer because of more direct and more efficient charge transfer path.[8] Therefore, we can observe intense research on TiO_2NT/conducting polymer heterojunctions and their application for photocurrent generation[9], water splitting[10] and energy storage.[11,12]

As a conducting polymer, polyaniline[13], polypyrrole[14] or poly(3,4-ethylenedioxythiophene)[15] are used. In most cases, polymer is formed inside the TiO_2NTs *via* electrochemical[16] or photoelectrochemical polymerisation.[17] Depending on the polymerisation conditions (potentiostatic, potentiodynamic) and titania morphology, polymer matrix can be introduced inside the tubes or deposited on the outer wall.[18] Furthermore, there have also been some attempts in order to facilitate and make deposition of polymer more uniform. Mainly it concerns titania modification by silane derivatives[19] or electrode illumination during the polymerisation process[16] (photoelectrochemical polymerisation). However, titania nanotubes obtained by anodization has fairy high resistance which hampers direct electrodeposition of conducting polymer and additionally an insulating barrier layer present between titanium metal plate and tubular nanostructure[20]. In recent times, in order to achieve improved

conductivity of TiO_2, and ultimately to achieve effective polymer deposition, hydrogenation treatment was proposed.[21] According to the literature reports, TiO_2 treatment in hydrogen atmosphere enhances electrochemical activity and conductivity due to increased donor density and introduction of surface hydroxyl groups.[22,23] Thus, such an approach could lead to activating the titania surface in order to enable its further electrochemical modifications.

This paper focuses on the formation of composite material containing ordered titania nanotubes infiltrated with conducting polymer: pEDOT:PSS. Titanium nanotubes were formed onto the titanium foil via anodization in fluoride rich electrolyte, followed by calcination in order to obtain crystalline phase of materials. Anatase NTs were subjected to hydrogen plasma in order to activate the surface for further polymer deposition. The introduction of polymer inside the nanostructure was realized by potentiostatic electropolymerization when Ti/TiO_2NTs acts as a working electrode immersed in monomer and counter ion solution. The morphology, crystal structure and composition were investigated using scanning electron microscopy, Raman, UV-vis and X-ray photoelectron spectroscopy techniques. Electrochemical activity of composite electrode as well as pure and hydrogenated titania was tested by means of cyclic voltammetry and electrochemical impedance spectroscopy measurements. In order to verify the stability of TiO_2NTs/polymer junction under illumination, long transient photocurrent measurements were performed.

EXPERIMENTAL

Preparation of hydrogenation TiO_2

The TiO_2NTs samples were prepared via two-step anodization according to the previously optimized procedure.[24] Before anodization, the substrate sample (Ti plate, Steam, 99.7%) was ultrasonically cleaned in the following order: in acetone, ethanol and water for 10 minutes in each solvent, and ultimately dried in air. The process was realized in a two-electrode configuration at room temperature, where the titanium plate served as an anode and the platinum mesh as a cathode with a fixed distance of 2 cm between them. The first anodization took place in the electrolyte containing: ethylene glycol (EG), 0.27 M NH_4F and 1 vol. % of deionized water. Anodization was performed at 40 V for 2 h, with the initial voltage rate of 0.1 V/s. Then, the titanium plate was immersed for 12 h in 0.5% wt. solution of oxalic acid in order to first remove the rugged nanotube layer. The second anodization process was performed on the as-cleaned titanium plate under the same conditions as those during the first anodization. In order to remove surface debris, the titanium plates covered with nanotubes

were immersed in 0.05% wt. HF for 180 s. After second anodization, the samples were rinsed with deionised water, dried in air and thermally treated at 450°C for 2 h with a heating rate of 2°C/min to transform the amorphous TiO_2 into a crystalline phase.

Finally, TiO_2NTs were subjected to a hydrogen environment in a plasma reactor (Electronic Diener) operating at power of 40 W, at room temperature, for 60 min. The obtained sample was coded as H-TiO_2NTs.

Fabrication of H-TiO_2NTs/PEDOT-PSS

Electrochemical polymerization was carried out to prepare H-TiO_2NTs/PEDOT:PSS. After a series of optimization experiments, electrochemical deposition was performed in an aqueous solution containing 0.1 M NaPSS and 0.001 M EDOT, by a potentiostatic polymerization of 1.6 V vs. Ag/AgCl/0.1 M KCl consuming charge of 30 mC cm^{-2}. The hydrogenated titania sample constituted a working electrode. The reference electrode was Ag/AgCl/0.1 M KCl, and a platinum mesh was used as a counter electrode. Finally, the working electrode was washed with deionized water and dried in air.

Characterization

The surface morphology and cross-section were examined using the Schottky field emission scanning electron microscopy (FEI Quanta FEG 250) with an ET secondary electron detector. The beam accelerating voltage was kept at 10 kV. For elemental analysis, the Energy Dispersive X-ray Spectroscopy (EDX) was performed by EDAX Genesis APEX 2i with ApolloX SDD spectrometer in a particular area of each sample. In order to confirm uniform polymer deposition, the elemental analysis was completed on the surface and across the composite layer. The chemical nature of elements and binding properties of the surface was studied using the X-ray photoelectron spectroscopy (XPS), by means of the Escalab 250Xi from ThermoFisher Scientific. High-resolution spectra were recorded at the energy step size of 0.1 eV at a pass energy of 10 eV. In order to normalize the spectroscopic measurements, the X axis (binding energy, E_{bin}) from XPS spectrum was calibrated for peak characteristics of neutral carbon 1s (E_{bin} = 284.6 eV). The UV-Vis reflectance spectra of titania nanotubes were measured with a dual beam UV-Vis spectrophotometer (Lambda 35, Perkin-Elmer) equipped with a diffuse reflectance accessory. The spectra were registered in a range of 300 - 700 nm, with a scanning speed of 60 nm/min. Bandgap energy values were determined as the intercept of the tangent of the plot of transformation of the Kubelka-Munk function. This method was used to designate the

bandgap energy for pure and H-TiO_2NTs. The Raman spectra were recorded by a confocal micro-Raman spectrometer (InVia, Renishaw) with sample excitation, by means of an argon ion laser emitting at 514 nm operating at 5% of its total power (50 mW).

Electrochemical and photoelectrochemical measurements

Electrochemical measurements were carried out using an AutoLab PGStat 302N potentionstat-galvanostat system (Methrom, Autolab) in the standard three-electrode assembly, where titanium foil covered by nanotubes served as a working electrode (active surface area of 0.3 cm^2). Electrodes were tested in contact with deaerated aqueous 0.5 M K_2SO_4 electrolyte. An electrochemical cell was equipped with a quartz window. The photoactive layers were illuminated with a 150 W Xenon lamp (Osram XBO 150) and an AM 1.5 filter was used to obtain simulated solar light and the automated light chopper with a period of 90 s was used as a light source. The irradiance of incident light was measured to be 100 mW/cm^2 using a reference cell (Si solar cell, Rera). The photocurrent measurements were carried out at + 0.5 V *vs*. Ag/AgCl/0.1M KCl bias voltage. In order to perform measurements under the visible light range, an additional cut-off optical filter ($\lambda > 420$ nm) was added to the experimental setup.

Electrochemical impedance spectroscopy (EIS) measurements for titania as well as composite samples were conducted at the frequency range between 20 kHz and 0.1 Hz, covering 75 points and with 10 mV amplitude of the AC signal. In order to perform the Mott-Schottky analysis, impedance spectra were recorded at different potentials in the range between +0.9 V and - 0.6 V *vs*. Ag/AgCl/0.1M KCl. Before each spectra registration, the potential was held to achieve a steady state condition. The impedance data were analysed on the basis of an electric equivalent circuit (EEQC) using an EIS Spectrum Analyser program.

RESULTS AND DISCUSSION

Characterisation

Scanning electron microscopy was employed to investigate the surface morphology of H-TiO_2 NT and composite H-TiO_2NTs/pEDOT:PSS. Fig. 1 a and b shows the top-view and cross-section SEM image of pure and H-TiO_2NTs layer, respectively. The obtained nanotubes were ordered and aligned. When comparing the SEM images registered for both materials, no difference was observed in the nano-architecture between the hydrogenated and pure titania. This suggests clearly that the applied plasma treatment did not influence the morphology and

only potential changes in the chemical states could have an impact on the electrochemical properties of titania. High resolution images allows to determine tube dimensions: internal diameter of 100 nm, a tube-wall thickness - 25 nm and tube length - 2.5 μm. In Fig. 1 c, the layer of titania nanotubes infiltrated with pEDOT:PSS is presented. The images demonstrate the growth of polymer film on the surface as well as along the tubes. In some cases, the holes are entirely filled with pEDOT:PSS matrix. This type of layer growth allows for a close metal oxide - polymer contact, which is required in the p-n heterojunction photovoltaic cells. Furthermore, in order to determine the location of deposited polymer, the obtained composite H-TiO_2NTs/pEDOT:PSS was immersed in diluted hydrofluoric acid (0.5 M) that selectively dissolves TiO_2 nanotubes.[25] The efficiency of crystalline titania form removal was proven by Raman spectrum where no bands typical for anatase was registered. After the removal of the titania network acting as polymer scaffolding, pEDOT:PSS collapses and does not retain the ordered structure (see, Fig. 1 d). The observed shape of remaining polymer allows us to conclude that polymerization takes place both inside and in-between nanotubes as previously observed by Janáky et al.[26]

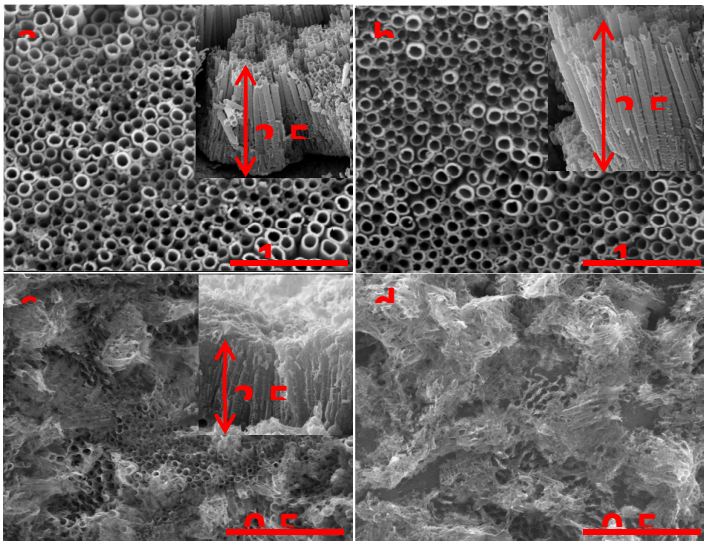

Fig. 1 The SEM images of a) pure TiO_2, b) hydrogenated TiO_2, c) H-TiO_2NTs/pEDOT:PSS composite material d) remaining pEDOT:PSS after H-TiO_2 removal

Energy dispersive X-ray spectroscopy was used to study the distribution of the polymer matrix over the titania surface and along the tubes. As shown in Fig. S1 a-c, it can be clearly seen that the distribution of elements (C, O, S) included into pEDOT:PSS is homogeneous

Therefore, the material composition is preserved when the sample was investigated at its surface. The atomic content of each element present in the composite sample is as follows: Ti: 33.04 at%; O: 51.23 at%, C: 15.01 at%, S: 0.36 at%. Knowing that polymer also contains oxygen atoms, the titanium to oxygen ratio deviates from TiO_2 stoichiometry that suggest oxygen deficit in the inorganic semiconductor. Furthermore, the local EDX analysis performed in nine different points across composite materials (see Fig. S2) proved uniform distribution of sulphur that builds pEDOT:PSS and oxygen and carbon species present in polymer and titania material as well. Thus, it could be concluded that polymer penetrates the free space in the titania nanostructure from the surface region down to the tube base. However, because EDX inspection is characterized by limited resolution, the further investigations with the use of XPS was carried out under the etching mode allowing more valuable analysis, as it will be shown in next paragraph.

The Raman spectra recorded for composite material and its pure counterparts: hydrogenated titania nanotubes and conducing polymer are shown in Fig. 2. As a reference, Raman spectra for unmodified titania nanotubes are given. A number of bands characteristic for the pure anatase crystalline form of TiO_2 were distinguished in the samples of pristine titania and composite material. The bands located at 144, 198, 395, 516 and 637 cm^{-1} are attributed to $E_{g(1)}$, $E_{g(2)}$, B_{1g}, A_{1g}, B_{1g} and $E_{g(3)}$ active anatase modes, respectively.[27,28] Characteristic bands of pEDOT:PSS are observed for pure polymer and composite material. The main band at 1433 cm^{-1} can be assigned to symmetric (C = C)-O bond vibrations in the thiophene ring. Two peaks at 1495 cm^{-1} and 1561 cm^{-1} could be interpreted as asymmetric C = C modes in polymer chains.[29] The peaks 1366 and 1267 cm^{-1} are characteristic for vibrations of single bonded carbon atoms in the polymer chain and in the thiophene ring, respectively. The oxyethylene ring deformations can be identified at 988, 571 and 442 cm^{-1}.[30] The Raman spectra registered both for the pure titania and hydrogenated sample are very similar. This indicates that the material has not changed significantly during the plasma treatment. However, as it is presented in Fig. 2b, a slight shift of $E_{g(1)}$ maximum from 143.3 cm^{-1} registered for pure TiO_2NTs to 145.7 cm^{-1} for H-TiO_2NTs is observed. This shift can be attributed to the increased amount of oxygen vacancies in H-TiO_2.[31] Furthermore, the zoomed–in view of the Raman spectra reveals that $E_{g(1)}$ peak of hydrogen plasma treated titania is broadened compared to those of pure TiO_2. Such spectral broadening arises most likely from the modification[32] of the crystal lattice resulted from oxygen vacancy formation. Such oxygen vacancy defects are known to play important role in absorption of O_2 molecules

or could act as electron scavenger leading to retardation of charge recombination. The intensity of anatase signal $E_{g(1)}$ of the H-TiO_2NTs is also much higher than that of pure TiO_2, which demonstrates that the crystal size of TiO_2 may be increased by hydrogen plasma treatment.[33,34] Nevertheless, according to Samsudin et al.,[34] the larger role in improved electrical properties of hydrogenated titania is played by Ti^{3+} and oxygen vacancies rather than the surface disorder or change in crystal size created during hydrogenation process.

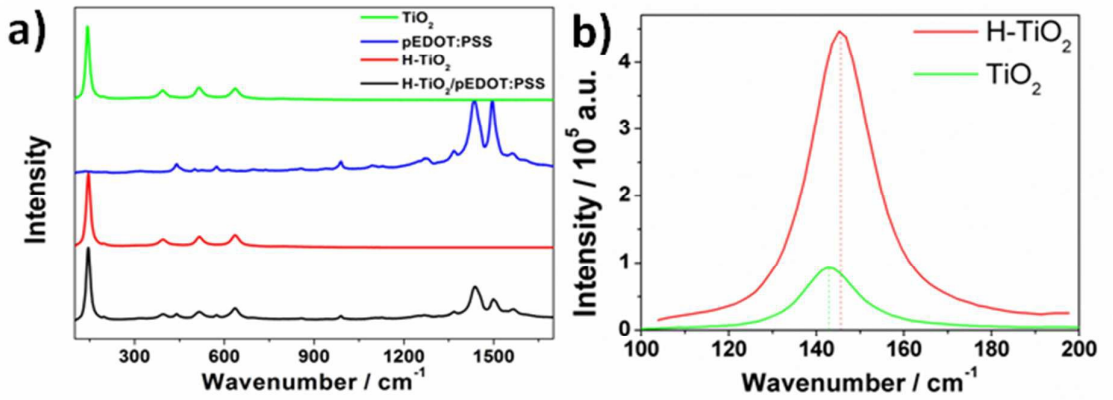

Fig. 2 (a) Raman spectra of pristine and hydrogenated titania, pEDOT:PSS film and composite material, (b) the zoomed-in view of the $E_{g(1)}$ peak for pristine and hydrogenated TiO_2.

UV-Vis spectroscopy was also used to characterize the optical properties of the obtained materials. Additionally, it determined the energy band gap for H-TiO_2 and TiO_2 nanotubes. In Fig. 3a and 3b, the absorbance curves and the plot of Kubelka-Munk function *vs.* photon energy are presented, respectively. Moreover, the typical absorption in the UV region[35], the broad band in the range of 400-600 nm was registered for both pure and H-TiO_2 NTs, but the absorbance ability of hydrogenated titania is much higher when compared to pure TiO_2. The values of E_{bg} determined on the basis of the Tauc plot are 3.08 and 2.98 eV for pure and H-TiO_2 NTs, respectively. The narrowing of bandgap energy was discussed in detail by Wang et al.[36] Upon hydrogenation, the titania disorder shell loses lattice periodicity and breaks the octahedral symmetry of TiO_6, and a tail of the conduction band (CB) is formed which leads to bandgap narrowing. Furthermore, surface defects and reconstruction in titania nanocrystals lead to strong band tailing near the CB edge, whereas hydrogen atoms introduce localized states below the CB minimum. To summarize, the enhancement of absorbance in a visible region results from electronic transitions from the tailed conduction band, localized states of oxygen vacancies as well as from mid-gap electronic states to the conducting band.

For the pEDOT:PSS modified sample, the broad and intensive band between 500-700 nm is observed that results from the presence of polymer matrix.[37] The increase in the absorbance ability of heterojunction in the visible range results from the occurrence of π-π* transitions[38] in the oxidized polymer matrix. The run of the absorbance curve registered for H-TiO_2NTs/pEDOT:PSS indicates that the composite material should exhibit better photoactivity under visible light than its pure counterparts, therefore, it is especially useful for application in photovoltaic cells. Change in absorbance properties exhibited after polymer deposition is also clearly visible as a deep blue colour of composite material (see Fig. S3).

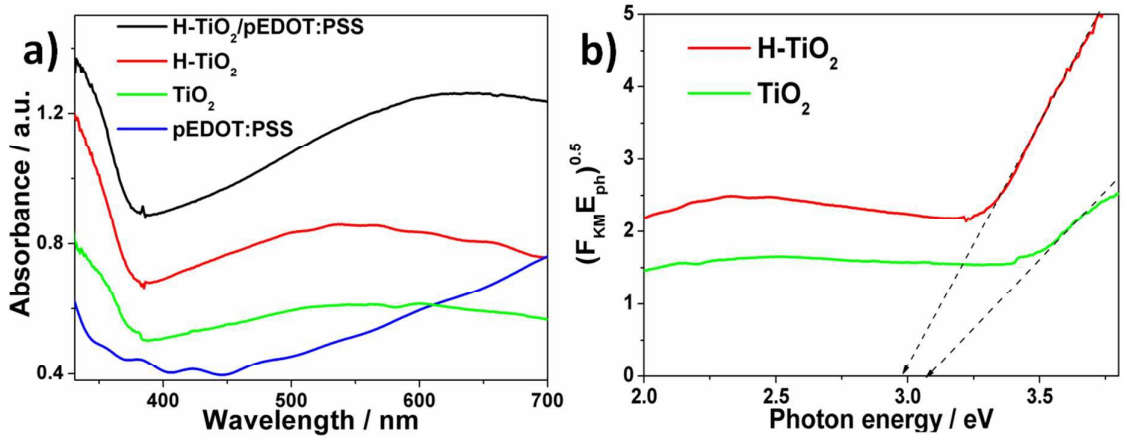

Fig. 3 a) Absorbance spectra for titania nanotubes and composite material, b) the Tauc plot for pure and hydrogenated TiO_2NTs.

In order to investigate the change in the chemical state of elements upon hydrogen plasma treatment, X-ray photoelectron spectroscopy measurements were performed. The XPS spectra recorded for titanium, oxygen and carbon region for hydrogenated titania are shown in Fig. 4, while Table 1 gives the position of each spectra maxima. The respective spectra found for pure titania were described in our previous report.[39] On the contrary to unmodified TiO_2, the region attributed to titania for H-TiO_2 is characterized as two doublets containing both Ti2$p_{1/2}$ and Ti2$p_{3/2}$ signals. The highest maxima located at 459.07 eV is attributed to Ti(IV) in anatase crystalline phase.[40] However, this value is shifted by 0.29 eV when compared to the respective peak recorded for pure titania The small peaks at 457.20 eV for Ti2$p_{3/2}$ and 462.62 eV for Ti2$p_{1/2}$ result from the existence of Ti(III).[41] The relation between the atomic content of Ti(IV) and Ti(III) equals 14.2:1. The appearance of Ti(III) state is typical for samples treated in hydrogen plasma and suggests that oxygen vacancies are formed to maintain electrostatic balance.[20]

Concerning the oxygen region, the registered O1*s* signal could be fitted by two single peaks located at 530.30 and 531.11 eV. The highest one results from lattice oxygen Ti-O[42] and is located at lower binding energy when compared to the pure sample. This probably results from the change in the oxidation state of partial titania species linked with oxygen atoms. The second peak found at 531.11 eV could be attributed to oxygen vacancy - Ti(III) type surface states.[43] According to Wang et al.[44], oxygen vacancies play a critical role in the visible light absorption, and therefore the absorbance ability of H-TiO_2 is improved in comparison to pure TiO_2.

As it was registered for pure TiO_2, a signal assigned to carbon species was also found for a hydrogenated sample. The C1*s* spectra were deconvoluted into three singlets with maxima located at 284.81 eV, 286.03 eV and 289.22 eV. The first peak is typical for C-C bonds. According to the literature, the presence of such carbon species results from surface contamination originating from an anodization process performed in an organic electrolyte[1] or from the XPS instrument itself.[45] The second and third signal could be assigned to carbon linked to oxygen by single[46] and double bonds[47], respectively.

As it was mentioned, the series of XPS measurements were performed with simultaneous etching of composite layers (see Fig. S4). At the surface area, where polymer covers TiO_2NT, both signals attributed to oxygen and sulphur atoms reaches their maximum value. After subsequent etching of H-TiO_2NTs/pEDOT:PSS, the atomic content of S and O atoms decreases with simultaneous increase of signal attributed to titania species. However, from the 3h up to the end of etching procedure, the atomic content of S, Ti and O does not change significantly that clearly revealed that the pEDOT:PSS matrix fill in interior of H-TiO_2NTs layer and three dimensional inorganic-organic interface is formed.

Table 1. The binding energies of core levels: Ti2*p*, O1*s* and C1*s* elements present in hydrogenated titania nanotube arrays.

orbital	symbol	E_{bin} / eV	at. %
C1*s*	**A**	284.81	10.31
	B	286.33	3.00
	C	289.22	1.29
Ti2*p*	**Ti2$p_{3/2}$ A**	459.07	23.62
	Ti2$p_{1/2}$ A	464.79	-
	Ti2$p_{3/2}$ B	457.20	1.66
	Ti2$p_{1/2}$ B	462.62	-
O1*s*	**A**	530.30	40
	B	531.11	20.05

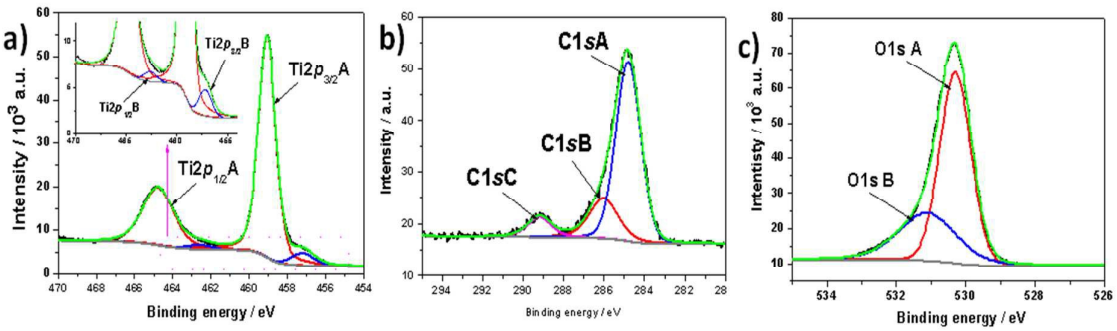

Fig. 4 High resolution XPS spectra recorded at the (a) titanium, (b) oxygen and (c) carbon for H-TiO_2 nanotubes.

Electropolymerisation analysis

As was mentioned in the experimental section, the deposition of conducting polymer was realized via potentiostatic electrochemical polymerisation. The chronoamperometry curves for electropolymerization of pEDOT:PSS over a pure and hydrogenated titania layer are shown in Fig. 5. As it can be seen, a huge difference in the current density value and its shape was observed. In the case of hydrogenated titania, an increase in the current is registered at the initial stage. Within about 15 s a current plateau typical for already overlapped nuclei of a new phase is achieved. Finally, the whole polymerisation process is realized within only 60 s. This may result from a short nucleation time.[48,49] In the case of pure titania, an exponential current decay is observed. The shape of the current, which changes with time, is typical for early stages of polymerisation, before nuclei are overlapped.[50] At the potential of 1.6 V vs. Ag/AgCl/0.1M KCl, the electropolymerisation occurs inefficiently on pristine titania and the extended time range of pEDOT:PSS deposition is needed for polymer film formation.[51] Despite electropolymerisation on pure TiO_2 was carried out for an hour the uniform polymer deposition was not achieved and it unable comparison of electrochemical and photoelectrochemical properties between H-TiO_2/pEDOT:PSS and TiO_2/pEDOT:PSS composite.

In contrast, electrode oxidation on H-TiO_2 is fully realized by charge propagation and leads to the formation of a conducting polymer film. Thus, the hydrogenation process could activate the titania surface and facilitate monomer absorption, nucleation and the whole electropolymerisation would occur efficiently. However, to prove changes in adsorption conditions upon plasma treatment, further studies are required. At this stage of our

investigation one may postulate that facilitation may result from a significant impedance decrease resulting from hydrogenation, as described in the following chapter.

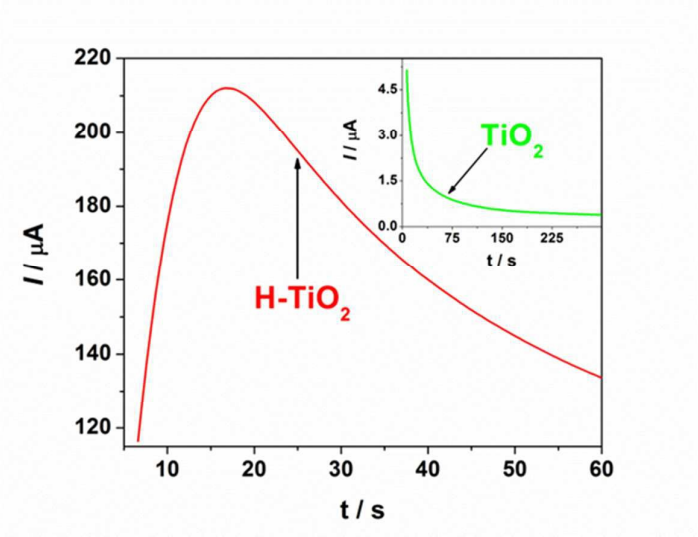

Fig. 5 Current time transients for pEDOT:PSS electropolymerisation at pure and hydrogenated TiO_2NTs at registered at E = 1.6 V *vs*. Ag/AgCl/0.1M KCl (electrolyte: aqueous solution of 0.1 M NaPSS and 0.001 M EDOT)

Electrochemical characterisation of hydrogenated titania

The cyclic voltammetry curves registered for pure and hydrogenated titania are given in Fig. 6. In the investigated potential range, both samples deliver obvious pseudocapacitive characteristics that could be attributed to the oxidation/reduction of surface hydroxyl groups.[20] The observed low electrochemical activity of unmodified titania could be due to its high resistance.[52] The reduction peaks at around 0 V *vs*. Ag/AgCl/0.1M KCl can be ascribed as an activity of intraband gap localized states.[53] In contrast to pure TiO_2NTs upon hydrogen plasma treatment, the charging current density increases significantly, which is related with the capacitance enhancement and conductivity improvement.[20,54]

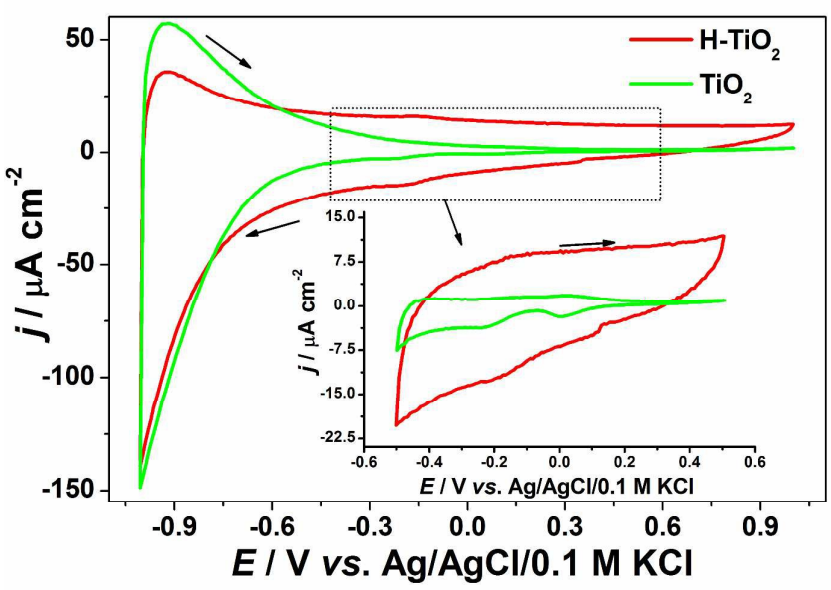

Fig. 6 Cyclic voltammetry curves recorded for pristine and hydrogenated titania immersed in 0.5M K_2SO_4, v = 50 mV s^{-1}.

In order to investigate sample resistance, electrochemical impedance measurements were conducted on pristine and hydrogenated titania materials. The spectra were collected at the rest potential as well as in the wide potential range. As it is shown in Fig. 7, the spectra exhibit at least two time constants attributed to the response of the space charge layer in series with the Helmholtz layer at the electrolyte side. This concept state was proposed as a base for an analysis of obtained spectra and an electric equivalent circuit (EEQC) given in Fig. S5 together with value of each parameter listed in Table S1. Same EEQC was previously applied for pure and non-metal doped titania[25] and is similar to proposed by other researchers.[55,56] The goodness of the performed fitting procedure was of the order of 10^{-5}. The meaning of each element was given in one of our last report and also in electronic supplementary information.

When comparing the spectra registered at the open circuit potential (E_{OCP}), the enormous decrease in R_1 resistance of H-TiO_2 in comparison to an untreated sample is observed, which suggest that charge transfer processes between tubular film and titanium support will be facilitated. The value of CPE_1 element does not change much upon hydrogenation, whereas the value of CPE_2 element increases by two orders of magnitude. The inconsiderable increase of capacitance attributes to the bottom, planar oxide film is related to its low real surface area and electrochemical activity. On the other hand, the enlargement of tubular oxide capacity denoted for H-TiO_2 could be explained in terms of higher donor concentration and anodic shift of the flatband potential when compared to pure TiO_2[53] as shown later.

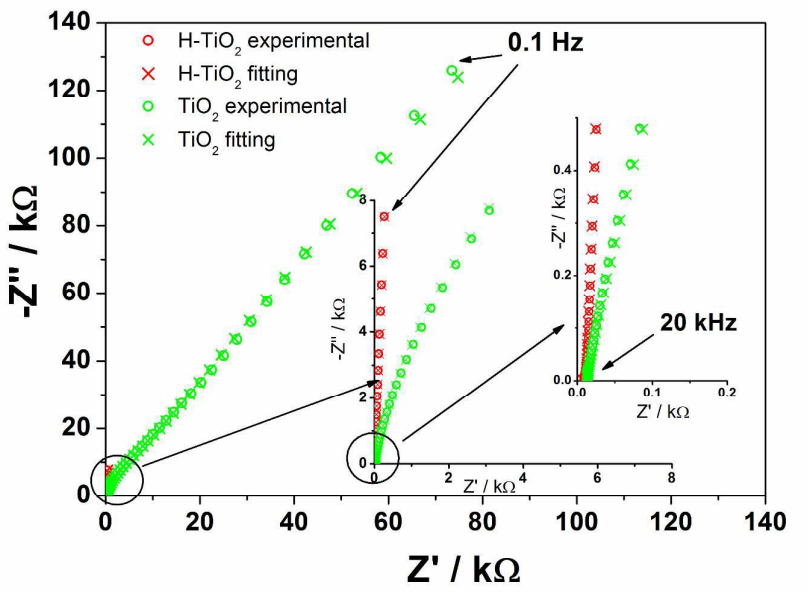

Fig. 7 Impedance spectra regstered for TiO_2 and H-TiO_2 nanotubes at the open circuit potential: E_{OCP} (TiO_2NTs) = +0.33 V, E_{OCP} (H-TiO_2NTs) = -0.09 V *vs*. Ag/AgCl/0.1M KCl (electrolyte: 0.5M K_2SO_4).

The analysis of the impedance spectra recorded in the wide potential range allows us to perform an analysis according to the Mott-Schottky relation given as:

$$\frac{1}{C^2} = \left(\frac{2}{q\varepsilon\varepsilon_0 N_D}\right)\left(E - E_{fb} - \frac{kT}{q}\right) \quad (4)$$

where C is a real capacity of the space charge layer, q – elementary charge, ε_0 – vacuum permittivity, ε - dielectric constant, N_D - concentration of donors, E - applied potential bias, E_{fb} – flatband potential, k - Boltzmann's constant, T – absolute temperature. The run of the Mott-Schottky plot both for pristine and hydrogenated titania is shown in Fig. S6 and it shape was discussed in detail in our previous work.[25] The nonlinear relation in the range between +0.6 and -0.9 is due to intrinsic electronic state[53], and could result from charging of bulk or surface states[57] or the irregular inhomogeneous distribution of O^{2-} ions.[58] The positive slope exhibited by both titania samples is characteristic for n-type semiconductor and from the intercept with E-axis flatband potential could be determined.[59] For pure titania, E_{fb} equals -0.2 V *vs*. Ag/AgCl/0.1M KCl, whereas in the case of H-TiO_2, E_{fb} value is cathodically shifted to +0.1 V *vs*. Ag/AgCl/0.1M KCl. Such an upward shift of flatband potential could lead to larger band bending at the surface of H-TiO_2 and could facilitate separation of charge carriers at electrode/electrolyte interface[60] that will considerably affect the overall photoconversion

efficiency. The difference of slopes of the two plots is also observed and indicates a huge disparity of donor densities in pure and modified titania. The carrier density N_D could be calculated from the following equation:

$$N_D = (2/e\varepsilon\varepsilon_0)\left[\frac{dC^{-2}}{dE}\right]^{-1} \quad (5)$$

when the following values are taken into account: e = 1.6 × 10^{-19}, ε_0 = 8.86×10^{-14} F/cm, and ε = 31 for anatase.[61] The calculated donor densities of TiO_2NTs and H-TiO_2NTs are 6.45×10^{20} and 2.27×10^{23} cm^{-3}, respectively. Despite the Mott-Schottky plot not allowing for estimation of the absolute value of N_D[62], the significant difference shows that upon hydrogen plasma treatment donor the density is greatly enhanced when compared to unmodified samples. Such change was observed for other hydrogenated titania and is commonly attributed to the introduction of substantial oxygen vacancies that are regarded as electron donors in titania.[63,64] Therefore, H-TiO_2 is characterized with better conductivity, and therefore improved charge separation and transport within the material could be expected.

Electrochemical properties of the composite material

Electrochemical studies also consider composite material and cyclic voltammetry as well as the electrochemical impedance spectroscopy measurements performed. CV curves and the registered impedance spectra at the open circuit potential are shown in Fig. 8 and Fig. 9, respectively. The working electrode was polarized from the rest potential in the anodic direction up to 0.7 V and back up to -0.7 V *vs*. Ag/AgCl/0.1M KCl. Among tested materials, only the composite electrode exhibits symmetrical cathodic/anodic current peaks at +0.15 *V vs.* Ag/AgCL/0.1M KCl and significantly higher current density when compared to that recorded for H-TiO_2 nanotube or pure polymer film, which illustrates improved electrochemical activity. The electrochemical impedance measurements performed on the composite material show its hybrid nature between pure polymeric and titania material. The shape of registered spectra for H-TiO_2NT/pEDOT:PSS is similar to that of pEDOT:PSS alone[65], but the resistance is higher due to titania network presence. The EEQC proposed for titania samples was modified by the introduction of additional arrangement of elements attributed to the polymer part (see Fig. S7). The goodness of the proposed fitting equals 6.5×10^{-5}, whereas the values for each element of EEQC were listed in Table S2. When conducting polymer is present, the electronic conductivity of the whole composite results not only from the titania network, but also from charge propagation along the oxidized pEDOT chains. The action accruing at the oxidized chains could proceed according to the reactions[66]:

$pEDOT^{x+} + xe^- + PSS^- \rightarrow pEDOT + x(PSS^-)_{sol}$

and/or $pEDOT^{x+}(PSS^-)_x + xe^- + C^+ \rightarrow pEDOT(PSS^-)_x(C^+)_x$

The interpretation of the majority of elements was given in the section concerning impedance of H-TiO_2NTs. Here, R_3 is attributed to resistance at TiO_2 nanotube/polymer interface and CPE_3 reflects the pseudocapacitance of pEDOT:PSS.[67] Because of the capacitive character exhibited by infiltrated polymer, the overall capacitance of composite increases, which is in agreement with the shape of cyclic voltammetry curves. In summary, the registered impedance spectra show double nature of H-TiO_2NTs/pEDOT:PSS material and the impact of polymer on the improvement of composite electric properties is evident. The decrease of the overall resistance could play an important role in the transfer of photogenerated charge carriers.

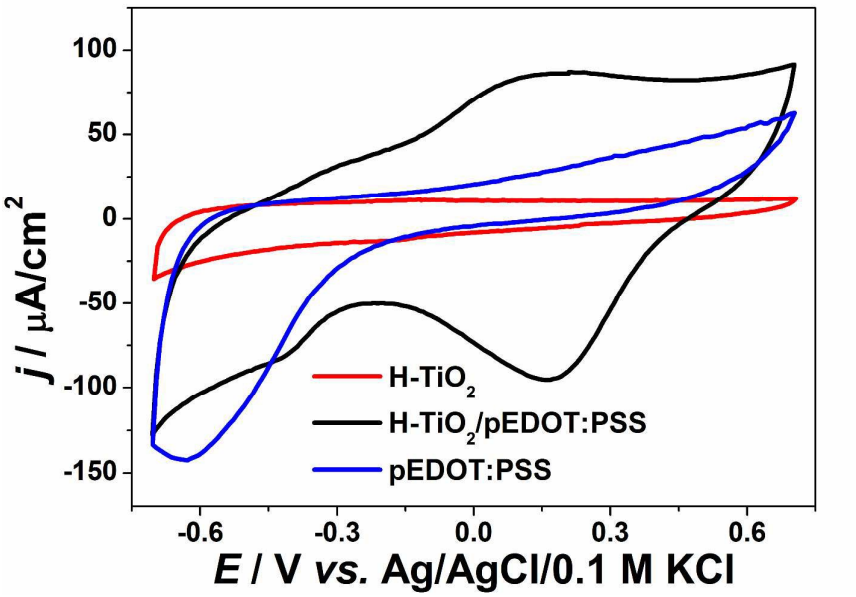

Fig. 8. The cyclic voltammetry curves of composite material H-TiO_2NTs/pEDOT:PSS and its pure counter parts (electrolyte: 0.5 M K_2SO_4, v = 50 mV s^{-1}).

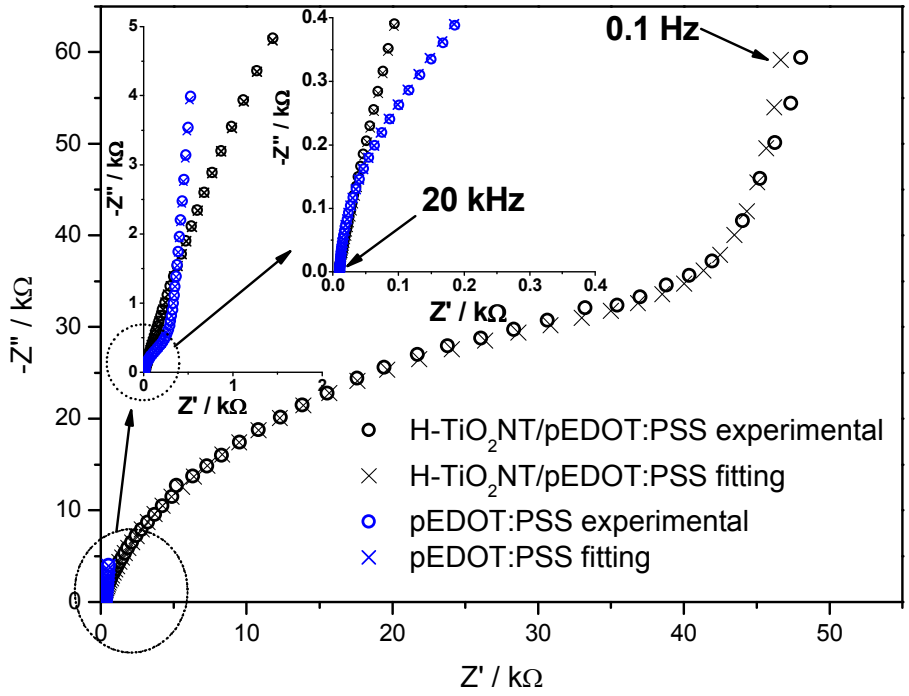

Fig. 9 Impedance spectra registered for pEDOT:PSS and composite material: H-TiO_2NTs/pEDOT:PSS at the open circuit potential: E_{OCP} (pEDOT:PSS) = +0.27 V, E_{OCP} (H-TiO_2NTs/pEDOT:PSS) = +0.24 V *vs.* Ag/AgCl/0.1M KCl (electrolyte: 0.5M K_2SO_4).

Photoelectrochemical activity

Photoelectrochemical properties of electrodes were investigated using the chronoamperometry technique recorded at the constant potential under "chopped" simulated solar light illumination. The materials obtained were anodically polarized (E = 0.5 V *vs.* Ag/AgCl/0.1 M KCl) and immersed in 0.5 M K_2SO_4 aqueous electrolyte without any additives acting as a hole capturer. The chronoamperometry curves of H-TiO_2NTs/pEDOT:PSS, and as reference: H-TiO_2NTs, TiO_2NTs and pEDOT:PSS layer, are presented in Fig. 10 and the values of photocurrent density registered after 8 min. of measurements are listed in Table 2.

Among all tested materials, conducting polymer alone exhibits the lowest photoactivity that is typical for neat PEDOT.[8,26] In the case of H-TiO_2 and TiO_2 nanotubes, after 8 min of measurement duration, the photocurrent density upon UV-vis irradiation reached 54 and 42 μA cm^{-2}, respectively. Thus, a hydrogenated sample is characterized with almost 30% enhancement that results from a higher absorbance ability and improved electric properties

when compared to pristine titania. It should also be noted that despite hydrogenation treatment, titania response upon illumination is stable and any current diminution is not observed. After the deposition of polymer, the obtained composite material is characterized by remarkable photoactivity, reaching ca. 106 μA cm^{-2} under UV–Vis illumination and 4.9 μA cm^{-2} when electrode is illuminated by vis radiation. The observed enhancement is significantly higher both under UV-Vis and Vis irradiation than that described for the heterojunction composed of pEDOT:PSS and titanium dioxide nanoparticles.[68] The improved photoactivity of H-TiO_2NTs/pEDOT:PSS in comparison to its pure counterparts results from formation of p-n heterojunction when appropriate alignment of conduction and valence band positions of both p-type and n-type semiconductor allows for charge separation at the organic/inorganic heterojunction[69]. According to Haring et al[70], in the case of conducting polymer-TiO_2 composite, there are three criteria of efficient hybrid bulk heterojunction: a) Fermi level of TiO_2 to be close to its conduction band, b) the difference between conduction band and LUMO should equal at least 0.3 eV[71] and c) Fermi level should be higher when compared to energy polarons level in the separated materials.[72]

Upon infiltration of titania by pEDOT:PSS, charge transfer from TiO_2 would create positive polarons in the polymer matrix, resulting in the formation of an electric field in the polymer that would assist photoelectron injection. Furthermore, in the case of oxygen vacancies presence, the excess of negative charge on Ti(III) sites leads to the formation of occupied deep traps below the conduction band.[73] As it was demonstrated, unlike pristine titania, the proposed hydrogenation treatment of TiO_2NTs results in partial reduction of Ti(IV) to Ti(III) and a decrease of the Fermi level of the flatband electrode that could allow for spontaneous electron transfer from pEDOT:PSS to H-TiO_2NTs. It should be noted that not only the favourable conditions for the formation of electron polarons in H-TiO_2NTs/pEDOT:PSS are responsible for photocurrent increase of in the p-n junction. Other factors, such as improved absorbance ability in the visible range when compared to titania NTs or pEDOT:PSS layer and ordered morphology of titania layer facilitating electron percolation and providing large contact area with polymer uniformly distributed on the surface as well as along the tubes, also play an important role in the enhancement of photoconversion efficiency.[74]

Additionally, the stability of H-TiO_2NTs/pEDOT:PSS upon prolonged illumination was also verified (see Fig. S8). In contrast with our previous results on TiO_2NTs/pEDOT:PSS heterojunction[14] or other titania-polymer heterojunctions,[75,76] even during 50 min of illumination, no drop of photoactivity was observed. It should also be noted that upon long-term irradiation, the current density value slightly increases this is due to oxidation of polymer

layer induced by photon absorption. The change in oxidation has an impact on the position of energy levels[77] and thus charge transfer at the organic/inorganic interface could proceed more efficiently. The electrochemical stability of composite material was confirmed before and after illumination using cyclic voltammetry measurements. As it is shown in Fig. S6 b, the shape of the CV curve remains unchanged - this confirms excellent photoresistivity of the organic-inorganic heterojunction.

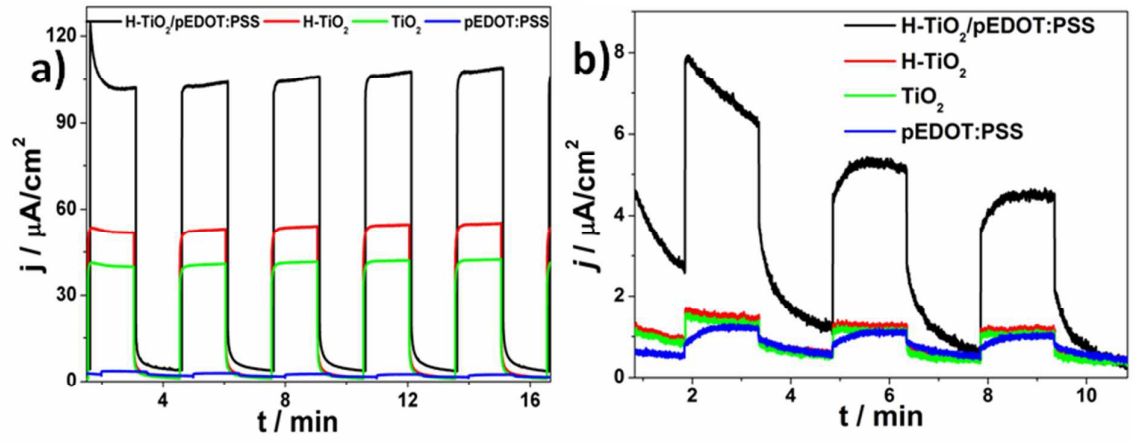

Fig. 10 Transient photocurrent response of pure and hydrogenated titania, pure polymer and H-TiO_2NT/pEDOT:PSS composite material registered under (a) UV-Vis and (b) vis illumination at 0.5 V *vs*. Ag/AgCl/0.1 M KCl (electrolyte: 0.5 M K_2SO_4).

Table 2. The photocurrent values obtained for investigated electrode materials under UV-Vis and vis illumination after 500 s of measurement.

Electrode material	*j* (UV-Vis) / μA cm^{-2}	*j* (Vis) / μA cm^{-2}
H-TiO_2NTs/pEDOT:PSS	106	4.9
H-TiO_2 NTs	54	0.9
TiO_2 NTs	42	0.8
pEDOT:PSS	2	0.7

Conclusions

In this paper, the conducting polymer pEDOT:PSS was used as organic sensitizer to form three dimensional heterojunctions with ordered titania nanotubes. The infiltration of titania with polymer was realized *via* electropolymerisation that was carried out on titania electrode followed by its treatment in hydrogen plasma. Spectroscopic and electrochemical measurements show that the proposed plasma processing leads to formation of Ti(III) species,

an enhancement of absorbance ability in the visible range, conductivity and capacitance improvement when compared to pristine TiO_2. On the basis of the impedance spectra analysis, flatband potential and donor density were estimated, and for TiO_2 E_{fb} = -0.16 V *vs*. Ag/AgCl/0.1M KCl, $N_D = 6.45\times10^{20}$ cm^{-3}, whereas for H-TiO_2NTs E_{fb} = +0.11 V *vs*. Ag/AgCl/0.1M KCl and $N_D = 2.27\times10^{23}$ cm^{-3}. A detailed elemental analysis has shown that hydrogen plasma facilitates uniform deposition of polymer matrix resulting in high surface area of organic-metal oxide interface. The obtained composite material exhibits much higher capacitive current when compared to its pure counterparts while registered impedance spectra reflects its duplex polymer-metal oxide nature. An appropriate alignment of energy levels of p- and n-element of H-TiO_2NTs/pEDOT:PSS heterojunction results in photocurrent density of 106 μA cm^{-2} under UV-vis and 4.9 under vis irradiation that is approx. 2 and 5.6 times higher when compared to that registered for H-TiO_2, respectively. To summarise, H-TiO_2NTs/pEDOT:PSS composite can be regarded as attractive material in the design of the photovoltaic cell with the possibility of forming a large p-n heterojunction.

ACKNOWLEDGMENTS

This work received financial support from the Polish National Science Centre: Grant No. 2012/07/D/ST5/02269.

References

1 P. Roy, S. Berger and P. Schmuki, *Angew. Chemie,* 2011, **50***,* 2904.
2 D. Kowalski, D. Kim and P. Schmuki, *Nano Today,* 2013, **8***,* 235.
3 D. Wang, Y. Liu, B. Yu, F. Zhou and W. Liu, *Chem. Mater*., 2009, **21**, 1198.
4 J. M. Macak, H. Tsuchiya, A. Ghicov, K. Yasuda, R. Hahn, S. Bauer and P. Schmuki, *Opin. Stat. Solid Mater. Sci*., 2007, **11**, 3.
5 B. Chen, J. Hou and K. Lu, *Langmuir,* 2013, **29**, 5911.
6 K. Siuzdak, M. Abbas, L. Vignau, M. Devynck, G. Dubacheva and A. Lisowska-Oleksiak, *J. Appl. Phys.,* **2012**, **112***,* 123110.
7 Q. Chen and D. Xu, *J. Phys. Chem. C*, 2009, **113**, 6310.
8 J. Boucle, P. Ravirajan and J. Nelson, *J. Mater. Chem*., 2007, **17**, 3141.
9 Y. Jia, P. Xiao, H. He, J. Yao, F Liu, Z. Wang and Y. Li, *Appl. Surf. Sci*., 2012, **258***,* 6627.
10 J. Luo, Y. Ma, H. Wang and J. Chen, *Electrochim. Acta,* 2015, **167**, 119.
11 P. M. Dziewoński and M. Grzeszczuk, *Electrochim. Acta,* 201**0**, **55**, 336.
12 G. F. Samu, C. Visy, K. Rajeshwar, S. Sarker, V. R. Subramanian and C. Janáky, *Electrochim. Acta,* 2015, **151**, 467.
13 S. H. Mujawar, S. B. Ambade, T. Battumur, R. B. Ambade and S. H. Lee *Electrochim. Acta,* 2011, **56**, 4462.
14 Y. Jia, P. Xiao, H. He, J. Yao, F. Liu, Z. Wang and Y. Li, *Appl. Surf. Sci*., 2012, **258**, 6627.
15 K. Siuzdak, M. Sawczak and A. Lisowska-Oleksiak, *Solid State Ionics,* 2015, **271**, 56.

16 H. Du, Y. Xie, C. Xia, W. Wang and F. Tian, *New J. Chem*., 2014, **38**, 1284.
17 C. Janaky, N. R. de Tacconi, W. Chanmanee and K. Rajeshwar, *J. Phys. Chem. C*, 2012, **116**, 19145.
18 D. Kowalski, and P. Schmuki, *Chem. Comm*., 2010, **46**, 8585.
19 S. Xie, M. Gan, L. Ma, Z. Li, J. Yan, H. Yin, X. Shen, Z. Xu, J. Zhang and J. Hu, *Electrochim. Acta,* 2011, **56**, 4462.
20 C. Janaky and K. Rajeshwar, Progress in Pol. Sci., 2015, 43, 96.
21 J. Chen, Z. Xia, H. Li, Q. Li and Y. Zhang, *Electrochim. Acta,* 2014, **120**, 408.
22 X. Lu, G. Wang, T. Zhai, M. Yu, J. Gan, Y. Tong and Y. Li, *Nanoletters,* 2012*,* **12**, 1690.
23 H. Wu, C. Xu, J. Xu, L. Lu, Z. Fan, X. Chen, Y. Song and D. Li, *Nanotechnology,* 2013, **24**, 455401.
24 K. Siuzdak, M. Szkoda, M. Sawczak, and A. Lisowska-Oleksiak, *New J. Chem*., 2015, **39**, 2741.
25 D. Kowalski and P. Schmuki, *RSC Adv.* 2013, **3***,* 2154.
26 C. Janáky, G. Bencsik, A. Racz and C. Visy, *Langmuir,* 2010, **26**, 13697.
27 K. Siuzdak, M. Szkoda, M. Sawczak, A. Lisowska-Oleksiak, J. Karczewski and J. Ryl, *RSC Adv.,* 2015, **5**, 50379.
28 X. Chen and S. S. Mao, *Chemical Reviews,* 2007, **107**, 2891.
29 A. Lisowska-Oleksiak, A. P. Nowak, M. Wilamowska, M. Sikora, W. Szczerba and C. Kapusta, *Synth. Met*., 2010, **160**, 1234.
30 S. Garreau, G. Louarn and J. Buisson, *Macromolecules,* 1999, **32**, 6807.
31 Z. Wang, C. Y. Yang, T. Q. Lin, H.Yin, P. Chen, D. Y. Wan, F. F. Xu, F. Q. Huang, J. H. Lin, X. M. Xie and M. H. Jiang, *Energy. Environ. Sci.,* 2013, **6**, 3007.
32 X. B. Chen, L. Liu, P. Y. Yu, S. S. Mao, X. Chen, L. Liu, Y. Y. Peter and S. S. Mao, *Science,* 2011, **331**, 746.
33. A. Sasinka, T. Singh, S. Wang, S. AMthur and R. Kraehnert, *J. Vac. Sci. Technol. A*, 2015, **33**, 01A152.
34 E. M. Samsudin, S. B. A. Hamid, J. C. Juan, W. J. Basirun and A. E. Kandjani, *Appl. Surf. Sci*., 2015, **359**, 883.
35 Y. Mizukoshi, N. Ohtsu and N. Masahashi, *Appl. Sur. Sci.,* 2013, **283**, 1018.
36 Z. Wang, C. Yang, T. Lin, H. Yin, P. Chen, D. Wan and M. Jiang, *Adv. Funct. Mater.,* 2013, **23**, 5444.
37 C. Janáky, G. Bencsik, A. Rácz, C. Visy, N. R. de Tacconi, W. Chanmanee and K. Rajeshwar, *Langmuir,* 2010, **26***,* 13697.
38 A. P. Nowak, M. Wilamowska and A. Lisowska-Oleksiak, *J. Solid State. Electrochem*., 2010, **14**, 263.
39 K. Siuzdak, M. Szkoda, A. Lisowska-Oleksiak, K. Grochowska, J. Karczewski and J. Ryl, *Appl. Surf. Sci*., 2015, **357**, 942.
40 Q. Zhang, Y. Li, E. A. Ackerman, M. Gajdardziska-Josifovska and H. Li, *Appl. Catal. A: Gen*., 2011, **400**, 195.
41 X. Jiang, Y. Zhang, J. Jiang, Y. Rong, Y. Wang, Y. Wu and C. Pan, *J. Phys. Chem. C,* 2012, **116**, 22619.
42 X. Zhou, B. Jin, S. Zhang, H. Wang, H. Yu and F. Peng, *Electrochem. Commun*., 2012, **19**, 127.
43 X. Wu, C. Xu, J. Xu, L. Lu, Z. Fan, X. Chen, Y. Song and D. Li, *Nanotechnology,* 2013, **24**, 455401.
44 G. Wang, H. Wang, Y. Ling, Y. Tang, X. Yang, R. C. Fitzmorris, C. Wang, J. Z. Zhang and Y. Li, *Nano Letters,* 2011, 11, 3026.
45 Y. Li, G. Ma, S. Peng, G. Lu and S. Li, *Appl. Surf. Sci*., 2008, **254**, 6831.
46 J. Yang, H. Bai, Q. Jiang and J. Lian, *Thin Solid Films,* 2008, **516**, 1736.

47 T. I. T. Okpalugo, P. Papakonstantinou, H. Murphy, J. McLaughlin and M. N. D. Brow, *Carbon,* 2005, **43**, 153.
48 J. Xia, N. Masaki, K. Jiang and S. Yanagida, *J. Mater. Chem.,* 2007, **17**, 2845.
49 A. A. Alamrio and R. L. Vieira, *J. Chil. Chem. Soc*., 2006, **51**, 971.
50 M. E. Lyons, *Polymeric Systems*, 1996, 297.
51 M. Graczyk-Zajac, S. Y. Vassiliev, M. A. Vorotynsev and G. A. Tsirlina, *J. Solid State Electrochem*., 2010, **14**, 2039.
52 F. Fabregat-Santiago, J. Mora-Seró, G. Garcia-Belmonte and J. Bisquert, *J. Phys. Chem. B,* 2003, **107**, 758.
53 G. Boschloo and D. Fitzmaurice, *J. Phys. Chem. B,* 1999, **103**, 2228.
54 H. Wu, D. Li, X. Zhu, C. Yang, D. Liu, X. Chen, Y. Song and L. Lu, *Electrochim. Acta,* 2014, **116**, 129.
55 A. G. Muñoz, Q. Chen and P. Schmuki, *J. Solid State Electrochem*., 2007, **11**, 1077.
56 Z. Zhang, Z. Zhou, S. Nie, H. Wang, H. Peng, G. Li and K. Chen, *J. Power Sources,* 2014, **267**, 388.
57 D. B. Bonham and M. E. A. Orazem, *J. Electrochem. Soc.,* 1992, **139**, 127.
58 X. Wang and J. Zhao, *Nanotech. IEEE Trans.,* 2014, **14**, 113.
59 K. Gelderman, L. Lee and S. W. Donne, *J. Chem. Educ*., 2007, **84**, 685.
60 C. Yang, Z. Wang, T. Lin, H. Yin, X. Lü, D. Wan and M. Jiang, *J. American Chem. Soc.,* 2013, **135**, 17831.
61 H. Tang, K. Prasad, R. Sanjines, P. E. Schmid and F. Levy, F *J. Appl. Phys*., 1994, **75**, 2042.
62 B. Chen, J. A. Beach, D. Maurya, R. B. Moore and S. Priya,. *RSC Adv.,* 2014, **4**, 29443.
63 H. Cui, W. Zhao, C. Yang, H. Yin, T. Lin, Y. Shan, Y. Xie, H. Gu and F. Hang, *J. Mater. Chem. A,* 2014, **2**, 8612.
64 X. Lu, G. Wang, Z. Zhai, M. Yu, J. Gan, Y. Tong and Y. Li, *Nano Letters,* 2012, **12**, 1690.
65 A. Lisowska-Oleksiak and A. P. Nowak, *Solid State Ionics,* 2008, **179**, 72.
66 A. Lisowska-Oleksiak and A. Kupniewska, *Solid State Ionics,* 2003, **157**, 241.
67 H. Du, Y. Zie, C. Xia, W. Wang and F. Tian, *New J. Chem*., 2014, **38**, 1284.
68 J. Baek, Y. Kim and E. Kim, *Mol. Cryst. Liq. Cryst.,* 2008, **483**, 275.
69 A. Arena, N. Donato, G. Saitta, G. Rizzo, G. Neri and G. Pioggia, *J. Sol-Gel Sci. Techn.,* 2007, **43**, 41.
70 A. J. Haring, S. R. Ahrenholtz and A. J. Morris, *ACS Applied Mater. Interf*., 2014, **6**, 4394.
71 M. C. Scharber, D. Wuhlbacher, M. Koppe, P. Denk, C. W. Ardauf, A. J. Heeger and C. L. Brabec, *Adv. Mater*., 2006, **18**, 789.
72 S. Braun, W. R. Salaneck and M. Fahlman, *Adv. Mater*., 2009, **21**, 1450.
73 C. D. Valentin, G. Pacchioni and A. Selloni, *J. Phys. Chem. C*, 2009, **113**, 20543.
74 L. Bertoluzzi, L. Badia-Bou, F. Fabregat-Santiago, S. Gimenez and J. Bisquert, *J. Phys. Chem. Lett*., 2013, **4**, 1334.
75 Y. Jia, P. Xiao, H. He, J. Yao, F. Liu, Z. Wang and Y. Li, *Appl. Surf. Sci*., 2012, **258**, 6627.
76 X. Zhang, F. Peng, H. Wang, H. Yu and Y. Fang, *Chem. Comm*., 2011, **47**, 10323.
77 Y. Xinag, M. Qian, D. Guo and G. Zhang, *Chin. Phys. B,* 2014, **23**, 038504.

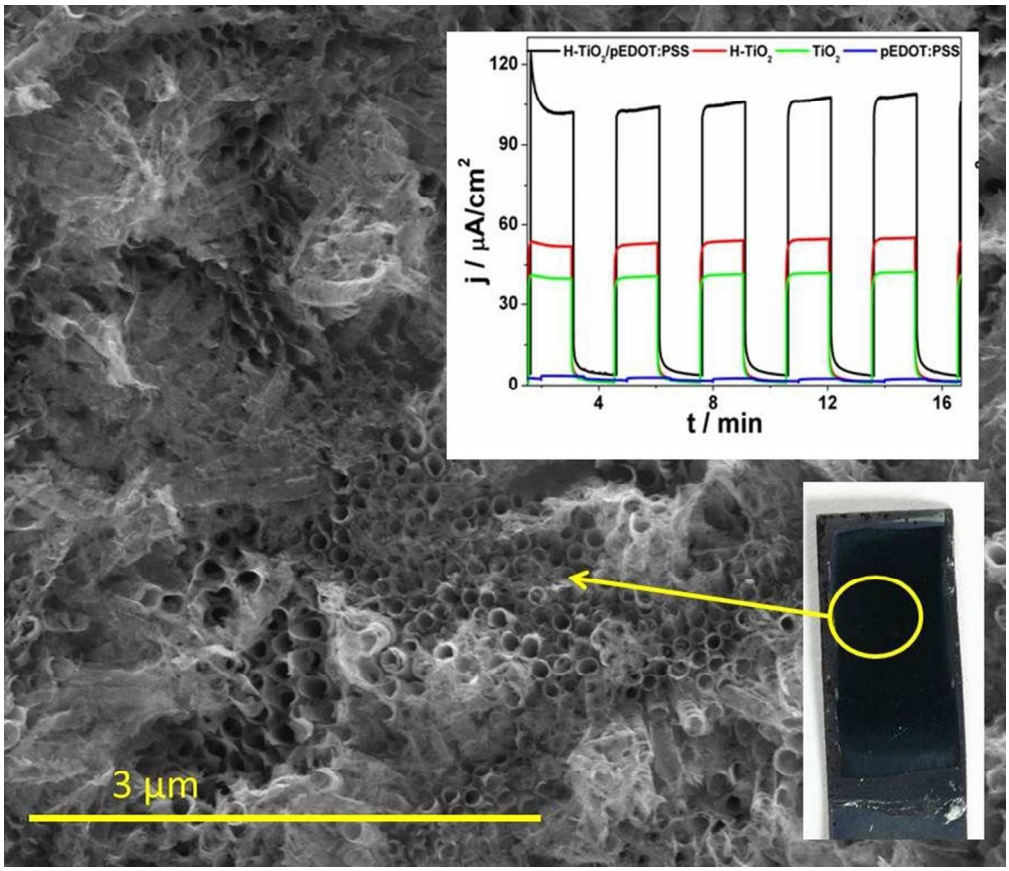

76x65mm (300 x 300 DPI)